would apply the second term of equation 1 to a postpeak current to calculate the initial surface coverage on the electrode surface, it would be determined as about 4.1×10^{-9} mol/cm^2. It corresponds to about 16 monolayers and about 66 Å thickness as before. The fact that the peak separation is about 27 mV larger than that in KNO_3 means that the redox reaction of ferricyanide/ferrocyanide at the electrode in sulfuric acid medium is less electrochemically reversible and less mobile than in KNO_3.

The preparation of ferricyanide layer on the gold electrode surface on the acidic medium yields a considerable thickness of multilayer which is behaving well in the electrochemical environments. This layer is even strongly molded in an acidic supporting electrolyte than in a neutral. The protons are known to bound to the nitrogen atoms of the CN groups of the ferrocyanide ion with intermolecular hydrogen bonding in the solid phase.[12] The origin of interactions which are responsible for adsorption or binding of ferricyanide to the gold surface in the self-assembly manner is not clearly understood yet, Brønsted interactions mediated by protons or Lewis interactions through Lewis acid site on the surface is one of the prospects.[13] To account for the formation of a multilayer on the surface, the interactions between monolayers should be addressed. Right now, from our experimental results we could propose a possibility of the proton-mediated hydrogen bonding between monolayers to generate a well-behaving multilayer of ferricyanides on the gold surface.

References

1. (a) Rubinstein, I.; Steinberg, S.; Tor, Y.; Shanzer, A.; Sagiv, J. *Nature* **1988**, *332*, 426. (b) Cheng, Q.; Brajter-Toth, A. *Anal. Chem.* **1992**, *64*, 1998. (c) Yang, H. C.; Aoki, K.; Hong, H.-G.; Sackett, D. D.; Arendt, M. F.; Yau, S.-L.; Bell, C. M.; Mallouk, T. E. *J. Am. Chem. Soc.* **1993**, *115*, 11855. (d) Chen, C. C.; Wei, C.; Rajeshwar, K. *Anal. Chem.* **1993**, *65*, 2437.
2. Wopschall, R. H.; Shain, I. *Anal. Chem.* **1967**, *39*, 1514.
3. (a) Wopschall, R. H.; Shain, I. *Anal. Chem.* **1967**, *39*, 1527. (b) Hulbert, M. H.; Shain, I. *Anal. Chem.* **1970**, *42*, 162.
4. Brown, A. P.; Anson, F. C. *Anal. Chem.* **1977**, *49*, 1589.
5. Cox, J. A.; Kulesza, P. J. *Anal. Chem.* **1984**, *56*, 1021.
6. (a) Ellis, D.; Eckhoff, M.; Neff, V. D. *J. Phys. Chem.* **1981**, *85*, 1225. (b) Krishnan, V.; Xidis, A. L.; Neff, V. D. *Anal. Chim. Acta* **1990**, *239*, 7. (c) Gao, Z.; Zhou, X.; Wang, G.; Li, P.; Zhao, Z. *Anal. Chim. Acta* **1991**, *244*, 39. (d) Moon, S. B.; Kim, Y. I. *Bull. Korean Chem. Soc.* **1995**, *16*, 511.
7. Lee, C.-K.; Kim, H.-S.; Lee, N.-S. submitted for publication.
8. Bard, A. J.; Faulkner, L. R. *Electrochemical Methods Fundamentals and Applications*; John Wiely & Sons, Inc.: New York, 1980; p 218 and p 521.
9. Zhang, D.; Wilson, G. S.; Niki, K. *Anal. Chem.* **1994**, *66*, 3873.
10. Huheey, J. E.; Keiter, E. A.; Keiter, R. L. *Inorganic Chemistry Principles of Structure and Reactivity*, 4th Ed.; Harper Collins, 1993; p 114.
11. Mullen, K.; Carron, K. *Anal. Chem.* **1994**, *66*, 478.
12. Cotton, F. A.; Wilkinson, G. *Advanced Inorganic Chemistry*, 4th Ed.; Wiley-Interscience: New York, 1980; p 755.
13. Simpson, S. F.; Harris, J. M. *J. Phys. Chem.* **1994**, *94*, 4649.

Ab Initio Study of Rare Gas-Hydrogen Ionic Cluster R_2H^+ (R=He, Ne, Ar)

Soon Tai Kim and Jae Shin Lee

Department of Chemistry, College of Natural Sciences, Ajou University, Suwon 441-749, Korea

Received August 8, 1995

The simple rare gas-hydrogen ionic clusters of R_2H^+ (R =He, Ne, Ar) are interesting species in that they represent the prototype of weakly bound (De~10 kcal/mole) molecular ions with the valence-active hydrogen which can serve as a medium to form more complex clusters. The formation of several rare gas-hydrogen molecular ions such as R_nH^+ (R=He, Ne, Ar; $n=1, 2, 3, 4$) in gas phase and in inert rare gas matrices can be facilitated not only by polarization forces between interacting partners but also by the special role proton can provide between essentially non-attractive rare gas atoms.[1] There have been many experimental and theoretical studies indicating the existence of stable rare gas-hydrogen ionic species.[2~18] In a collision experiment between R_2^+ and H_2 using flowing afterglow technique,[3] Adams, Bohme and Ferguson observed that either RH^+ or R_2H^+ could be dominant species in rare gas-hydrogen mixture in gas phase, depending upon hydrogen gas flow rate and rare gas ions. Although there have been a number of theoretical investigations on diatomic rare gas-hydrogen ionic species, there have been a few studies on triatomic and more complex ionic species, especially for Ne and Ar species, probably due to the number of electrons involved in the calculation and, more importantly, their non-valent (non-octet) electronic structures.

The most extensive theoretical study on R_2H^+ has been carried out by Matcha *et al.* based on *ab initio* Hartree-Fock Self-Consistent-Field (HF-SCF) calculations.[12~14] They calculated the equilibrium geometry and binding energy for these species as well as vibrational frequencies. They found that all species have linear symmetric equilibrium geometry ($D_{\infty h}$) and concluded that the bonding is basically due to the combination of charge induced dipole attractions resulting from the polarization of the rare gas atoms by the relatively unshielded proton charge and the repulsive exclusion forces resulting from the overlapping of the charge clouds centered on the rare gas atoms for He and Ne species. For Ar species, their results are unreliable due to the incompleteness of the basis set used in the calculation. More recently, Last and George[19] suggested the equilibrium geometry of Ar_2H^+ to be slightly bent and unsymmetrical, based on semiempirical diatomics in ionic systems (DIIS) method.[20,21] However,

Table 1. Total energies[a] of He_2H^+ in linear symmetric geometries

R_{He-H}[b]	HF[c]	MP2[c]
0.921	−5.8092155	−5.8814993
0.922	−5.8092219	−5.8815019
0.923	−5.8092269	−5.8815030[e]
0.924	−5.8092304	−5.8815027
0.925	−5.8092325	−5.8815010
0.926	−5.8092333[e] (−5.810168)[d]	−5.8814979
0.927	−5.8092327	−5.8814935
0.928	−5.8092307	−5.8814876

[a]Energies in atomic unit. [b]Bond length in Å. [c]Basis set is 6-311++G(3df,3pd). [d]Value in parentheses is the minimum energy by Matcha *et al.* (ref. 12). [e]Minimum energy at respective level.

Table 2. Total energies[a] of Ne_2H^+ in linear symmetric geometries

R_{Ne-H}[b]	HF[c]	MP2[c]
1.125	−257.1542572	−257.6970082
1.126	−257.1542595	−257.6970288
1.127	−257.1542610[e]	−257.6970477
1.128	−257.1542597	−257.6970651
1.129	−257.1542576	−257.6970810
1.130	−257.1542540	−257.6970953
.....	.....	.....
1.137	−257.1541891	−257.6971529
1.138	−257.1541743	−257.6971552
1.139	−257.1541581	−257.6971561[e]
1.140	−257.1541406	−257.6971555
1.141	−257.1541271	−257.6971536
.....	.....	.....
1.143	−257.1540801 (−257.17827)[d]	−257.6971454

[a]Energies in atomic unit. [b]Bond length in Å. [c]Basis set is 6-311++G(3df,3pd). [d]Value in parentheses is the fitted minimum energy by Matcha *et al.* (ref. 13). [e]Minimum energy at respective level.

neither Hartree-Fock nor semiempirical method are expected to give the accurate geometry or binding energy for this sort of weakly bound ionic clusters. In this paper, we report the results of large basis set, correlated calculations of R_2H^+ based on Møller-Plesset Perturbation Theory (MPPT).[22] The calculations were carried out using Gaussian 92.[23] MPPT is a size consistent method and the potential surface obtained at the level of second order correction of MPPT(MP2) without correction of basis set superposition error (BSSE)[24] was found to give very accurate ro-vibrational spectral transition lines for diatomic rare gas-hydrogen ionic species.[18] Thus the geometry was optimized at MP2 level and dissociation energy was obtained up to fourth order (MP4) with the standard basis set of 6-311++G(3df,3pd). This basis set, which is the largest one provided by Gaussian 92, includes the polarization and diffuse functions for heavy and light atoms, respectively, as well as triple zeta valence functions.

Table 3. Total energies[a] of Ar_2H^+ in linear symmetric geometries

R_{Ar-H}[b]	HF[c]	MP2[c]
1.496	−1053.7720380	−1054.1991224
1.497	−1053.7720577	−1054.1991247
1.498	−1053.7720798	−1054.1991260[e]
1.499	−1053.7720935	−1054.1991259
1.500	−1053.7721095	−1054.1991247
.....	.....	.....
1.511	−1053.7722066	−1054.1990357
1.512	−1053.7722084	−1054.1990209
1.513	−1053.7722090[e]	−1054.1990050
1.514	−1053.7722085	−1054.1989880
1.515	−1053.7722069	−1054.1989700
.....	.....	.....
1.587	−1053.7690874 (−1053.680)[d]	−1054.1943242

[a]Energies in atomic unit. [b]Bond length in Å. [c]Basis set is 6-311++G(3df,3pd). [d]Value in parentheses is the minimum energy by Matcha *et al.* (ref. 14). [e]Minimum energy at respective level.

Table 4. Single point energy[a] at different levels of theory

method	He_2H^+	Ne_2H^+	Ar_2H^+
HF	−5.8092269	−257.1541581	−1053.7720798
MP2	−5.8815030	−257.6971561	−1054.1991260
MP4	−5.8938686	−257.7138533	−1054.2503676
CCD[b]	−5.8939160	−257.6979717	−1054.2340158
QCISD(T)[c]	−5.8944361	−257.7120354	−1054.2508918

[a]Energy at MP2 optimized geometry in units of hartree. [b]Double substitution coupled cluster method. (ref. 33-35). [c]Quadratic configuration interaction method. (ref. 36).

The geometry was initially optimized using medium size basis set such as 6-31G(d,p). After that, geometries near minimum energy were scanned using larger basis set. From our results of geometry optimization, it was found that all species have a linear symmetric equilibrium geometry ($D_{\infty h}$) which is in accord with the results of Matcha *et al.*,[12~14] but in disagreement with the semiempirical results of Last and George.[19] In Table 1 through Table 3, we give the total energies of each species at several geometries near minimum at HF and MP2 levels. The energy change from HF to MP2 level is significant considering the binding energy of these species. Our results of HF minimum energies are slightly different from the ones by Matcha *et al.* This is due to, in some part, the difference in basis set size, and, in another part, inaccuracies in their minimum energies which were obtained by parabolic extrapolation for Ne and Ar species. In Table 4, we give the energies at various levels at the MP2 optimized geometry. Although the MP2 energy could be slightly lowered by using the correlation methods at higher levels such as MP4 or QCISD(T), the energy change is much smaller compared to the change between HF and MP2 level. In Table V, we give the equilibrium geometry

Table 5. Bond length and binding energy of RH^{+a} and R_2H^{+b} at equilibrium geometry[c]

	Bond length[d]			Binding energy[e]		
	HF	MP2	Expt.	HF	MP2	MP4[f]
HeH^+	0.771	0.773	0.774[g]	44.61	46.37	46.81
NeH^+	0.970	0.989	0.991[h]	50.53	53.26	53.81
ArH^+	1.271	1.277	1.28[i]	90.62	94.24	95.91
He_2H^+	0.926	0.923		11.40	13.13	13.30
Ne_2H^+	1.127	1.139		12.83	17.36	17.56
Ar_2H^+	1.513	1.498		8.65	16.20	15.54

[a]Binding energy is the energy difference between RH^+ and $R+H^+$. [b]Binding energy is the energy difference between R_2H^+ and RH^++R. [c]Same basis set(6-311++G(3df,3pd)) is used for all species. [d]Bond length in Å. [e]Binding energy in kcal/mole. [f]MP4/6-311++G(3df,3pd)//MP2/6-311++G(3df,3pd) result. [g]From ref. 5. the equilibrium bond length was derived using accurate potential curve of Kolos and Peek (ref. 15). [h]From ref. 6. [i]From ref. 7.

Table 6. Charge distribution for RH^+ and RHR^+ at equilibrium geometry[a]

	Partial charge[b]	
	R	H
HeH^+	0.291	0.709
NeH^+	0.368	0.632
ArH^+	0.546	0.454
$HeHHe^+$	0.105	0.789
$NeHNe^+$	0.191	0.619
$ArHAr^+$	0.219	0.562

[a]MP2/6-311++G(3df,3pd) optimized geometry. [b]Based on Mulliken's population analysis.

for RH^+ and R_2H^+ with the binding energy for each species at HF, MP2, and MP4 levels. The equilibrium bond distances between R and H on the HF level are in good agreement with MP2 results and experimental results (where available), and they are much longer in triatomic species than diatomic species. This supports the explanation of interacting molecular orbital picture for the bonding in this kind of ionic species[1,25] that stabilization of the binding is caused by the bond stretching effect of middle proton which reduces the highest occupied antibonding orbital energy. While the binding energy at MP2 and MP4 levels are very close each other for all species, the binding energies at HF and MP2(4) levels are becoming very different as one goes from He to Ar species, demonstrating the effect of electron correlation. It is clear that the binding energy is much more sensitive to electron correlation than equilibrium geometry in these ionic clusters. For Ar_2H^+, the correlation effect is much larger than for He_2H^+ and Ne_2H^+ which substantially increases the binding energy at MP2(4) level compared to HF level for Ar species. It is interesting to note that Ar_2H^+ is slightly less strongly bound than Ne_2H^+ with respect to RH^+ and R dissociated states. This is in contrast to the slight increase of binding energy for Ne_2H^+ compared to He_2H^+. This result appears to be related to the much stronger bonding in diatomic ArH^+ (~96 kcal/mole) than in NeH^+ (~54 kcal/mole). The strong bonding in ArH^+ was caused by the substantial charge (or electron) delocalization between Ar and H atoms. In Table 6, we give the charge distribution for diatomic RH^+ and R_2H^+ species based on Mulliken's population analysis.[26,27] The total charge is much more delocalized in ArH than NeH^+ or HeH^+, and, as a result, charge induced dipole interaction in $ArH^+\cdots Ar$ would be less attractive than in $NeH^+\cdots Ne$ despite the larger polarizability of Ar atom than Ne atom. In the formation of He_2H^+ and Ne_2H^+, however, the charge distribution is similar in diatomic HeH^+ and NeH^+, and more polarizable Ne atom appears to make a little stronger bonding to RH^+ compared to He. Of course, there will also be certain amount of valence bonding in each triatomic species which cannot be neglected. Meanwhile, the charge distribution in triatomic RHR^+ becomes similar all together with the middle hydrogen holding more positive charge than rare gas atoms. Therefore, our results indicate that various factors should be considered to predict the relative stabilities of the bonding in these ionic clusters including valence, polarization, and in some cases, dispersion (van der Waals) forces as well as vibrational contribution.[19,28] Our results also suggest that the potential energy surface of Ar_2H^+ could be quite different from the potential energy surface of Ne_2H^+, which was found to be very close to the one of He_2H^+ except the nuclei mass.[12,13] It would be interesting to investigate the effect of vibrational zero point energy to binding in these clusters in light of the previous study on XHX (X=halogen atom) type molecules[29-32] which showed the possibility of "vibrational bonding" in such systems.

Acknowledgment. This work was supported by the grant from the Korea Science and Engineering Foundation.

References

1. Dykstra, C. E. *J. Mol. Struct. (THEOCHEM)* **1983**, *103*, 131.
2. Chupka, W. A.; Russell, M. E. *J. Chem. Phys.* **1967**, *49*, 5426.
3. Adams, N. G.; Bohme, D. K. ; Ferguson, E. E. *J. Chem. Phys.* **1970**, *52*, 5101.
4. Bondybey, V. E.; Pimentel, G. C. *J. Chem. Phys.* **1972**, *56*, 3832.
5. Dabrowski, I.; Herzberg, G. *N.Y. Acad. Sci.* **1977**, *38*, 14.
6. Wong, M.; Bernath, P.; Amano, T. *J. Chem. Phys.* **1982**, *77*, 693.
7. Klingbeil, R. *J. Chem. Phys.* **1972**, *57*, 1066.
8. Ram, R. S.; Bernath, P. F.; Brault, J. W. *J. Mol. Spectrosc.* **1985**, *113*, 451.
9. Carrington, A.; Kennedy, R. A.; Softley, T. P.; Fournier, P. G.; Richard, E. G. *Chem. Phys.* **1983**, *81*, 251.
10. Peyerimhoff, S. *J. Chem. Phys.* **1965**, *43*, 998.
11. Poshusta, R. D.; Siems, W. F. *J. Chem. Phys.* **1971**, *55*, 1995.
12. Milleur, M. B.; Matcha, R. L.; Hayes, E. F. *J. Chem. Phys.* **1974**, *60*, 674.
13. Matcha, R. L.; Milleur, M. B.; Meier, P. F. *J. Chem. Phys.* **1978**, *68*, 4748.

14. Matcha, R. L.; Milleur, M. B. *J. Chem. Phys.* **1978**, *69*, 3016.
15. Kolos, W.; Peek, J. M. *Chem. Phys.* **1976**, *12*, 381.
16. Bondybey, V.; Pearson, P. K.; Schaefer III, H. F. *J. Chem. Phys.* **1972**, *57*, 1123.
17. Deakyne, C. A.; Liebman, J. F.; Frenking, G.; Koch, W. *J. Phys. Chem.* **1990**, *94*, 2306.
18. Hirst, D. M.; Guest, M. F.; Rendell, A. P. *Mol. Phys.* **1992**, *77*, 279.
19. Last, I.; George, T. F. *J. Chem. Phys.* **1990**, *93*, 8925.
20. Last, I.; George, T. F. *J. Chem. Phys.* **1987**, *87*, 1183.
21. Last, I.; George, T. F. *J. Chem. Phys.* **1988**, *89*, 3071.
22. Moller, C.; Plesset, M. S. *Phys. Rev.* **1934**, *46*, 618.
23. Frisch, M. J.; Trucks, G. W.; Head-Gordon, M.; Gill, P. M. W.; Wong, M. W.; Foresman, J. B.; Johnson, B. G.; Schlegel, H. B.; Robb, M. A.; Replogle, E. S.; Gomperts, R.; Andres J. L.; Raghavachari, K.; Binkley, J. S.; Gonzalez, C.; Martin, R. L.; Fox, D. J.; Defrees, D. J.; Baker, J.; Stewart, J. J. P.; Pople, J. A. *Gaussian 92, Revision C*, Gaussian Inc.,Pittsburgh, PA, 1992.
24. Boys, S. F.; Bernardi, F. *Mol. Phys.* **1970**, *19*, 553.
25. Pimentel, G. C. *J. Chem. Phys.* **1951**, *19*, 446.
26. Mulliken, R. S. *J. Chem. Phys.* **1955**, *23*, 1833.
27. Mulliken, R. S. *J. Chem. Phys.* **1955**, *23*, 2338.
28. Lee, J. S.; Secrest, D. *J. Chem. Phys.* **1986**, *85*, 6565.
29. Truhlar, D. G.; Olson, P.; Parr, C. A. *J. Chem. Phys.* **1972**, *57*, 4479.
30. Manz, J.; Meyer, R.; Pollak, E.; Romelt, J. *Chem. Phys. Letters* **1982**, *93*, 184.
31. Manz, J.; Meyer, R.; Romelt, J. *Chem. Phys. Letters* **1983**, *96*, 607.
32. Manz, J.; Meyer, R.; Schor, H. H. R. *J. Chem. Phys.* **1984**, *80*, 1562.
33. Cizek, J. *Adv. Chem. Phys.* **1969**, *14*, 35.
34. Hurley, A. C. *Electron Correlation in Small Molecules*; Academic, New York, 1969.
35. Pople, J. A.; Krishnan, R.; Schegel, H. B.; Binkley, J. S. *Int. J. Quantum Chem.* **1978**, *14*, 545.
36. Pople, J. A.; Head-Gordon, M.; Raghavachari, K. *J. Chem. Phys.* **1987**, *87*, 5968.

$La_{1-x}Ce_xCoO_3$ Catalytic Electrode Effect in a Sealed-Off CO_2 Laser

Myung-Hun Kim and Ung-In Cho*

Department of Chemistry, Yonsei University, Seoul 120-749, Korea

Received August 22, 1995

When a CO_2 laser is operating, large portion of the CO_2 molecules in the discharge tube discomposed to CO and O_2. Thus in a sealed-off laser, the primary consideration is how to keep CO_2 concentration in the tube, which can be recovered by recombining the dissociated CO and O_2. One of the solutions is using catalytic electrode which functions both as electrode and catalyst. Perovskite-type oxides have been studied for technologically important characteristics, especially electrocatalysis and automotive catalysis.[1,2] Cobaltate perovskite is known to be good catalysis for the oxidation of carbon monoxide and to have a metallic conductivity.[3] $La_{1-x}Sr_xCoO_3$ and $Nd_{1-x}Sr_xCoO_3$ are good examples.[4,5,6] Especially $La_{1-x}Sr_xCoO_3$ have been investigated intensively for lasing performance even up to 3500 hours.[7] The catalytic effects on x values are mainly ascribed to the variation in ratio of Co^{4+}/Co^{3+} and oxygen vacancies by substitution of Sr^{2+}. The oxygen vacancies are created with O_2 desorption from the surface of catalyst which have unstable Co^{4+} changed into Co^{3+} by providing an electron.[8,9]

Instead of strontium, cerium is also known to have a good catalytic activity.[10] This time, the nonstoichiometric significance is tetravalent ion Ce^{4+} in the place of divalent ion Sr^{2+}. Thus it is worthwhile to investigate $La_{1-x}Ce_xCoO_3$ for the catalytic electrode effects in a sealed-off CO_2 laser in addition to analyzing the change of CO_2 concentration *in situ* during discharging by photoacoutic spectroscopy (PAS).[11]

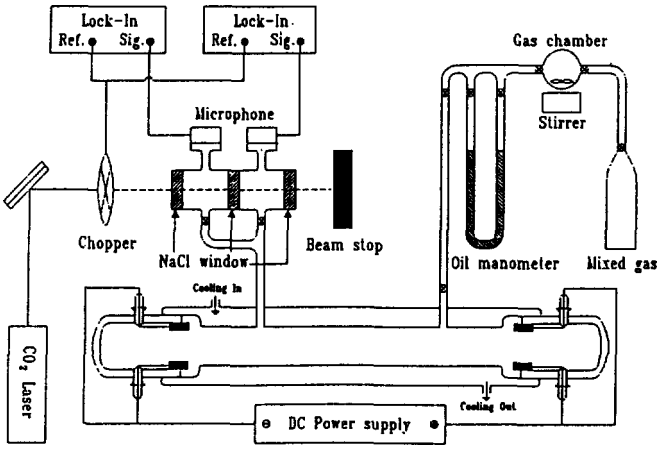

Figure 1. Diagram of experimental setup for the photoacoustic detection of CO_2.

Experiment

To investigate the catalytic electrode effect, experiments are arranged with a discharge tube with 16 mmϕ bore, 780 mm active length, and 157 cm^3 effective volume. Electrodes are adopted as a ring-type which was reported to have better performance in laser-output than a tablet-type. The ring-type electrodes of both cathode and anode has 26 mmϕ and 16 mmϕ external and internal diameter and 12-15 mm length. The diagram of the experimental set-up for the detection of CO_2 concentration *in situ* by PAS is shown in Figure 1. To monitor CO_2 concentration, a differential type photoacoustic cell is attached to the discharge tube. The output beam of cw CO_2 laser (Synrad 480), operating in multilines of 10.6 μm is modulated at 35 Hz by a light chopper, is directed into the differential cell. Two FET microphones are placed at the top of two photoacoustic cells to detect the change of acoustic pressure. The signals from the two microphones are monitored by two lock-in amplifiers (Stanford 510 and